Distributed Continuous-time Optimal Power Flow

Bishal Lamichhane[†], *Student Member, IEEE*, Yu Christine Chen[‡], *Member, IEEE*,
Roohallah Khatami[†], *Member, IEEE*
[†]Southern Illinois University, Carbondale, IL, USA, {bishal.lamichhane, roohallah.khatami}@siu.edu
[‡]The University of British Columbia, Vancouver, BC, Canada, chen@ece.ubc.ca

***Abstract*—In this paper, we propose a distributed continuous-time optimal power flow (OPF) model, with DC power flow constraints, for a multi-area transmission network. The model exploits the unique properties of variational optimization, function space representation, and the alternating direction method of multipliers (ADMM) to enable continuous-time power exchange between adjacent areas. More specifically, the centralized multi-area OPF is formulated as a variational optimization problem with continuous-time load and decision variables (power generation, voltage phase angles, line/tieline power flows), which is then converted to a conventional optimization problem by projecting the load and decision trajectories into the Bernstein function space, and is decomposed to function space-based OPF subproblems of individual areas using ADMM. The numerical results of implementing the proposed model on a synthesized three-area network indicate convergence to the centralized continuous-time OPF solution and showcase computational efficiency and the efficient sharing of ramping resources among areas.**

***Index Terms*—Optimal power flow, distributed optimization, continuous-time scheduling**

I. Introduction

Electric power grids are undergoing major changes mainly driven by integrating high levels of renewable energy, advancing energy storage technologies, and deploying electric vehicles at scale [1], [2]. Along with numerous benefits offered by this grid modernization, technical challenges also arise largely due to variability and uncertainty of renewable energy resources [3] as well as the stochastic nature of electric transportation charging demand [4]. To tackle these challenges, power system operators can tap into available operational flexibility from conventional generators and further equip additional flexibility resources (e.g., energy storage and flexible loads) along with institutional flexibility options (e.g., operational coordination of independently operated interconnected networks) [5]. Coordination of interconnected networks is indeed a viable source of operational flexibility, yet, to fully leverage the latent benefits we require to enhance the operation models and distributed coordination processes governing the power exchange among areas.

Due to the large number of electricity consumers of various types that may alter their power consumption at any time, the power system demand follows in reality a continuous-time trajectory. However, industry-standard power system operation models discretize this continuous-time load with zero-order piecewise constant functions and deploy the same type of functions to present the power generation schedule of generating units [6]. Although the zero-order approximation has hitherto served well, it may fail to reflect and address the sub-interval variations of renewable generation and the ensuing sharp changes in net load (load minus non-dispatchable renewable generation) [7]. In addition, this model defines the generation ramping as the finite difference of two consecutive generation values that overlooks the actual sub-interval ramping dynamics. Thereby, enhanced operation models with higher modeling flexibility are in demand. Function space-based discretization of load and generation trajectories is presented in [7] as an alternative solution and continuous-time operation models are developed to better reflect the net-load sub-interval variations and capture the generation ramping (defined as time-derivative of generation trajectories). This general method has since been applied to optimal scheduling of energy storage devices [8], stochastic flexibility reserve scheduling [9], dynamics-aware economic dispatch [10], regulation markets [11], hydro-thermal scheduling [12], and multi-energy system [13], [14]. However, to the best of our knowledge, *distributed* continuous-time multi-area scheduling has not yet been explored.

A large body of research has been dedicated to distributed optimization of electric power systems, albeit not with continuous-time decision trajectories [15]–[21]. In these, individual microgrids/areas typically share partial information on state variables of boundary buses (terminal buses of connecting lines) without sharing complete information on the internal generation fleet and network topology, thereby preserving privacy. In [15], a comprehensive review of distributed optimization techniques applied to optimal power flow (OPF) problem is presented. In [16], the analytical target cascading method is used to solve the OPF problem for a power distribution network. The auxiliary problem principle technique is utilized in [17] to solve a security-constrained economic dispatch, focused mainly on temporal decomposition of inter-temporal constraints. Dual decomposition is used in [18] to develop an incentive-compatible market coupling framework. Among the variety of distributed optimization algorithms, alternating direction method of multipliers (ADMM) has gained popularity due to favorable convergence properties [19]–[21]. The ADMM is used in [19] to enable trading congestion and imbalance mitigation services among distribution system operators, in [20] to optimally schedule the smart inverters of distributed energy resources, and in [21] for clearing energy and flexibility markets in community-based grids.

Distinct from the aforementioned work, in this paper, we propose a distributed *continuous-time* OPF model with DC power flow constraints, for a multi-area transmission network. We first formulate the centralized OPF problem as a variational

optimization problem that characterizes the nodal loads and power generation of online units, bus voltage phase angles, and line/tieline power flows, as continuous-time trajectories. Further, the sub-interval ramping dynamics is effectively captured via defining the generation ramping as time-derivative of power generation trajectories. The variational OPF problem is then approximated by projection into the Bernstein function space leading to a linear programming (LP) problem with Bernstein coefficients as decision variables. The ensuing LP is then decomposed into quadratic programming (QP) OPF subproblems of individual areas using the ADMM. Examined on a synthesized three-area test system, the solution of the proposed distributed continuous-time OPF problem accurately converges to that of centralized counterpart. Further, the generation and ramping resources are efficiently scheduled to not only supply the system load at minimum cost, but also address the ramping deficiency of areas with limited ramping resources by leveraging the excess ramping resources in other areas.

II. Methodology

Consider a power system with A areas contained in the set $\mathcal{A} = \{1, 2, \ldots, A\}$, where the topology data of area $a \in \mathcal{A}$ is conveyed through a directed graph $(\mathcal{N}_a, \mathcal{L}_a)$ such that $\mathcal{N}_a = \{1, 2, \ldots, N_a\}$ and $\mathcal{L}_a = \{(i,j)|i,j \in \mathcal{N}_a, j \equiv j(i)\}$ respectively represent the sets of nodes (buses) and edges (transmission lines). For area a, the continuous-time bus voltage angles and nodal loads form respectively the vectors $\theta_a(t) = [\theta_{a,1}(t), \theta_{a,2}(t), \ldots, \theta_{a,N_a}(t)]^{\mathrm{T}}$ and $D_a(t) = [D_{a,1}(t), D_{a,2}(t), \ldots, D_{a,N_a}(t)]^{\mathrm{T}}$, transmission line power flows are contained in vector $F_a(t) = [\big(F_{a,(i,j)}(t)\big)_{(i,j)\in\mathcal{L}_a}]$, and the $N_a \times N_a$ admittance matrix of each area is denoted by B_a. The set of K_a generating units at each area a is represented by $\mathcal{K}_a = \{1, \ldots, K_a\}$, the continuous-time power generation of units form the vector $G_a(t) = [G_{a,1}(t), G_{a,2}(t), \ldots, G_{a,K_a}(t)]^{\mathrm{T}}$, the continuous-time ramping trajectories which are the time-derivatives of power trajectories are represented by the vector $\dot{G}_a(t) = [\dot{G}_{a,1}(t), \dot{G}_{a,2}(t), \ldots, \dot{G}_{a,K_a}(t)]^{\mathrm{T}}$, and the $K_a \times N_a$ incidence matrix M_a maps the generating units to buses. Tielines connected to area a are collected in set $\mathcal{L}_a^{\mathrm{tie}} = \{(i,j)|i \in \mathcal{N}_a, j \in \mathcal{N}_{a'}, j \equiv j(i)\}$, the associated tieline power flows are contained in vector $T_a(t) = [\big(T_{a,(i,j)}(t)\big)_{(i,j)\in\mathcal{L}_a^{\mathrm{tie}}}]$, and the incidence matrix R_a maps the tielines to boundary buses. The above notation is illustrated via a generic multi-area power transmission network in Fig. 1. In this section, we formulate the centralized variational OPF problem followed by the pertinent function space representation. Application of ADMM to the resulting function space-based OPF problem then enables distributed solutions.

A. Centralized Variational OPF Problem Formulation

We formulate the centralized variational OPF problem in (1), where a single omniscient system operator has complete information regarding technical limitations and cost functions of generators as well as network topology of all areas and optimally operates the entire power system by using the available information. Nevertheless, we persist with notation for distinct areas and distinguish transmission line power flows from tieline power flows [22], as these facilitate formulating the distributed solution later. The operation cost of the power system integrated over the scheduling horizon $\mathcal{T}$ is minimized in (1a), subject to operation constraints in (1b)–(1i):

$$\underset{\Omega}{\text{minimize}} \quad \sum_{a\in\mathcal{A}} \int_{\mathcal{T}} C_a(G_a(t))dt, \tag{1a}$$

$$\text{subject to } B_a\theta_a(t) + R_aT_a(t) = M_aG_a(t) - D_a(t), \quad \forall a \in \mathcal{A},\ t \in \mathcal{T}, \tag{1b}$$

$$\underline{G}_a \le G_a(t) \le \overline{G}_a, \qquad \forall a \in \mathcal{A},\ t \in \mathcal{T}, \tag{1c}$$

$$\underline{\dot{G}}_a \le \dot{G}_a(t) \le \overline{\dot{G}}_a, \qquad \forall a \in \mathcal{A},\ t \in \mathcal{T}, \tag{1d}$$

$$F_{a,(i,j)}(t) = \frac{\theta_{a,i}(t) - \theta_{a,j}(t)}{x_{a,(i,j)}}, \quad \forall a \in \mathcal{A}, \ \forall (i,j) \in \mathcal{L}_a,\ t \in \mathcal{T}, \tag{1e}$$

$$T_{a,(i,j)}(t) = \frac{\theta_{a,i}(t) - \theta_{a',j}(t)}{x^{\mathrm{tie}}_{a,(i,j)}}, \quad \forall a \in \mathcal{A}, \ \forall (i,j) \in \mathcal{L}_a^{\mathrm{tie}},\ t \in \mathcal{T}, \tag{1f}$$

$$-\overline{F}_a \le F_a(t) \le \overline{F}_a, \qquad \forall a \in \mathcal{A},\ t \in \mathcal{T}, \tag{1g}$$

$$-\overline{T}_a \le T_a(t) \le \overline{T}_a, \qquad \forall a \in \mathcal{A},\ t \in \mathcal{T}, \tag{1h}$$

$$\theta_{1,1}(t) = 0, \qquad t \in \mathcal{T}, \tag{1i}$$

where $\Omega = \{G_a(t), \theta_a(t), F_a(t), T_a(t)\}_{t\in\mathcal{T},\ a\in\mathcal{A}}$ represents the set of decision trajectories, $C_a(G_a(t)) = \sum_{k\in\mathcal{K}_a} C_{a,k}(G_{a,k}(t))$ denotes the sum of convex cost functions of units in area a at time t, the vectors $\underline{G}_a$ and $\overline{G}_a$ respectively represent the minimum and maximum power generation limits, the vectors $\underline{\dot{G}}_a$ and $\overline{\dot{G}}_a$ contain the generation ramping limits, and the power flow limits of transmission lines and tielines are respectively collected in vectors $\overline{F}_a$ and $\overline{T}_a$. The nodal power balance is enforced through (1b) where the total transmission line/tieline power flows leaving each bus are equated to the injected power at the corresponding bus. The generation and ramping of units are constrained to their limits in (1c) and (1d), and transmission line and tieline power flows

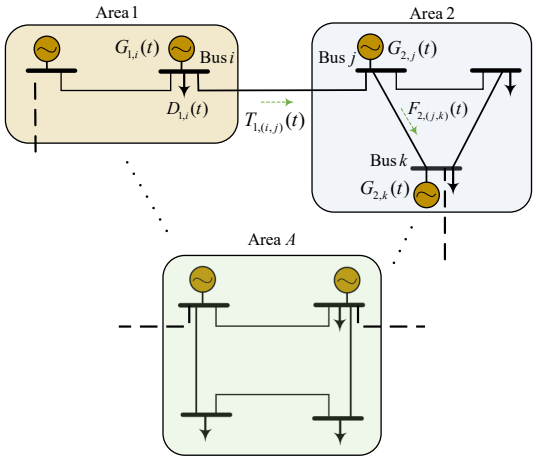

Fig. 1. Generic multi-area power transmission network.

are respectively calculated in (1e) and (1f) and confined to their thermal limits through (1g) and (1h), where $x_{a,(i,j)}$ ($x^{\text{tie}}_{a,(i,j)}$) represents line (tieline) reactance. Without loss of generality, the bus 1 of area 1 is designated as the system angle reference and its voltage phase angle is set to zero in (1i).

B. Bernstein Function Space

Let us subdivide the scheduling horizon $\mathcal{T}=[0,T]$ into S intervals $\mathcal{T}_s=[t_s,t_{s+1}),\rightarrow \mathcal{T}=\cup_{s=0}^{S-1}\mathcal{T}_s$ of the same length $\Delta = t_{s+1}-t_s = \frac{T}{S}$. For each interval $\mathcal{T}_s$, the continuous-time trajectories are projected into a Bernstein function space of degree Q, which basis functions are formed by the Bernstein polynomials of the same degree. By concatenating the basis functions attributed to individual intervals into a single vector of basis functions, we form a spline function space representing the entire scheduling horizon $\mathcal{T}$. This vector of basis functions is denoted by $e^Q(t)=[e^Q_1(t),\dots,e^Q_P(t)]^{\mathrm{T}}$ and includes $P=(Q+1)S$ functions defined as

$$e^Q_{s(Q+1)+q+1}(t) = b_{q,Q}\left(\frac{t-t_s}{T_s}\right), \quad t\in[t_s,t_{s+1}), \tag{2}$$

where $b_{q,Q}$ represents the q^{th} Bernstein polynomial of degree Q, $s=0,\dots,S-1$ and $q=0,\dots,Q$.

1) Decision Trajectories: For each area a, we project the power generation trajectories $G_a(t)$, bus voltage phase angles $\theta_a(t)$, transmission line power flows $F_a(t)$, and tieline power flows $T_a(t)$ into the function space spanned by $e^Q(t)$ as

$$G_a(t)=\mathbf{G}_a e^Q(t),\ \theta_a(t)=\boldsymbol{\theta}_a e^Q(t), \quad t\in\mathcal{T}, \tag{3}$$

$$F_a(t)=\mathbf{F}_a e^Q(t),\ T_a(t)=\mathbf{T}_a e^Q(t), \quad t\in\mathcal{T}, \tag{4}$$

where $\mathbf{G}_a$, $\boldsymbol{\theta}_a$, $\mathbf{F}_a$, and $\mathbf{T}_a$ are respectively $K_a\times P$, $N_a\times P$, $|\mathcal{L}_a|\times P$, and $|\mathcal{L}^{\text{tie}}_a|\times P$ matrices of Bernstein coefficients distinguished with bold symbols ($|\cdot|$ denotes the set cardinality).

2) Generation Ramping: The time-derivatives of generation trajectories, which are projected into a function space spanned by Bernstein polynomials of degree Q, are expressed in a Bernstein function space of degree $Q-1$ as follows:

$$\dot{G}_a(t)=\dot{\mathbf{G}}_a e^{Q-1}(t), \qquad t\in\mathcal{T}, \tag{5}$$

where $\dot{\mathbf{G}}_a$ is the $K_a\times(P-S)$ matrix of Bernstein coefficients that linearly relates to $\mathbf{G}_a$ through $P\times(P-S)$ matrix $\mathcal{M}$ as

$$\dot{\mathbf{G}}_a=\mathbf{G}_a\mathcal{M}. \tag{6}$$

3) Continuity of Trajectories: By imposing proper linear constraints on the Bernstein coefficients of decision trajectories corresponding to the adjacent intervals $s,\ s+1$, we ensure the continuity and smoothness in transitions between intervals. Please refer to [7] for a detailed discussion on continuity.

4) Objective Function: Suppose that the cost function of generator $k\in\mathcal{K}_a$, i.e., $C_{a,k}(G_{a,k}(t))$, is approximated with a piecewise linear function with $H_{a,k}$ linear, and correspond to each of the linear segments $h=1,\dots,H_{a,k}$ the positive auxiliary variable trajectories $g_{a,k,h}(t)$ and the segment lengths $\overline{g}_{a,k,h}$. Collect the auxiliary variable trajectories of all generators $k\in\mathcal{K}_a$ in vector $g_{a,h}(t)=[g_{a,1,h}(t),\dots,g_{a,K_a,h}(t)]^{\mathrm{T}}$ and the segment lengths in vector $\overline{g}_{a,h}$ likewise. By leveraging the unique properties of Bernstein polynomials [23], it is straightforward to convert the integral in the objective function (1a) to an algebraic function of Bernstein coefficients of decision trajectories as

$$\mathcal{J}_a = C_a\left(\underline{G}_a\right)T + \Delta\frac{\sum_{h=1}^{H_{a,k}}\mathbb{1}^{\mathrm{T}}_{K_a}\gamma_{a,h}\mathbf{g}_{a,k,h}\mathbb{1}_P}{Q+1}, \tag{7}$$

where $\mathbb{1}_{K_a}$ and $\mathbb{1}_P$ are respectively K_a- and P-dimensional vectors of ones, $\gamma_{a,h}$ is the $K_a\times K_a$ diagonal matrix of generator cost function slopes at the linearization segment h, and $\mathbf{g}_{a,h}$ is the $K_a\times P$ matrix of Bernstein coefficients of auxiliary variable trajectories.

5) Centralized Continuous-time Problem: With the above components in place, the centralized variational OPF problem in (1) is formulated in Bernstein function space as follows:

$$\underset{\boldsymbol{\Omega}}{\text{minimize}} \quad \sum_{a\in\mathcal{A}}\mathcal{J}_a \tag{8a}$$

$$\text{subject to } B_a\boldsymbol{\theta}_a + R_a\mathbf{T}_a = M_a\mathbf{G}_a - \mathbf{D}_a, \forall a\in\mathcal{A}, \tag{8b}$$

$$\underline{G}_a\mathbb{1}^{\mathrm{T}}_P \le \mathbf{G}_a \le \overline{G}_a\mathbb{1}^{\mathrm{T}}_P, \qquad \forall a\in\mathcal{A}, \tag{8c}$$

$$\underline{\dot{G}}_a\mathbb{1}^{\mathrm{T}}_{P-S} \le \mathbf{G}_a\mathcal{M} \le \overline{\dot{G}}_a\mathbb{1}^{\mathrm{T}}_{P-S}, \ \forall a\in\mathcal{A}, \tag{8d}$$

$$\mathbf{F}_{a,(i,j)} = \frac{\boldsymbol{\theta}_{a,i}-\boldsymbol{\theta}_{a,j}}{x_{a,(i,j)}}, \forall a\in\mathcal{A}, \forall(i,j)\in\mathcal{L}_a, \tag{8e}$$

$$\mathbf{T}_{a,(i,j)} = \frac{\boldsymbol{\theta}_{a,i}-\boldsymbol{\theta}_{a',j}}{x^{\text{tie}}_{a,(i,j)}}, \forall a\in\mathcal{A}, \forall(i,j)\in\mathcal{L}^{\text{tie}}_a, \tag{8f}$$

$$-\overline{F}_a\mathbb{1}^{\mathrm{T}}_P \le \mathbf{F}_a \le \overline{F}_a\mathbb{1}^{\mathrm{T}}_P, \qquad \forall a\in\mathcal{A}, \tag{8g}$$

$$-\overline{T}_a\mathbb{1}^{\mathrm{T}}_P \le \mathbf{T}_a \le \overline{T}_a\mathbb{1}^{\mathrm{T}}_P, \qquad \forall a\in\mathcal{A}, \tag{8h}$$

$$\boldsymbol{\theta}^{\mathrm{T}}_{1,1} = \mathbb{0}_P, \tag{8i}$$

$$\mathbf{G}_a = \underline{G}_a\mathbb{1}^{\mathrm{T}}_P + \sum_{h=1}^{H_{a,k}}\mathbf{g}_{a,h}, \qquad \forall a\in\mathcal{A}, \tag{8j}$$

$$\mathbb{0}_{K_a\times P} \le \mathbf{g}_{a,h} \le \overline{g}_{a,h}\mathbb{1}^{\mathrm{T}}_P, \qquad \forall a\in\mathcal{A}, \tag{8k}$$

$$\text{Continuity Constraints}, \tag{8l}$$

where $\boldsymbol{\Omega}=\{\mathbf{G}_a,\boldsymbol{\theta}_a,\mathbf{F}_a,\mathbf{T}_a\}_{a\in\mathcal{A}}$, $\mathbf{F}_{a,(i,j)}$ ($\mathbf{T}_{a,(i,j)}$) is the row of matrix $\mathbf{F}_a$ ($\mathbf{T}_a$) corresponding to line (tieline) (i,j), $\boldsymbol{\theta}_{a,i}$ is the row of matrix $\boldsymbol{\theta}_a$ corresponding to node i, and $\mathbb{0}_P$ ($\mathbb{0}_{K_a\times P}$) is the vector (matrix) of all zeros. Above, (8j) constructs the Bernstein coefficients of generation trajectories in terms of the Bernstein coefficients of pertinent auxiliary variables, while the auxiliary variable Bernstein coefficients are limited to linearization segments lengths in (8k). We refer interested readers to [8]–[10] for detailed exposition on function space representation, particularly the cost function linearization and the continuity constraints.

C. Distributed Continuous-time OPF Using ADMM

We formulate the distributed solution of the centralized OPF problem in (8) by using ADMM. To this end, we introduce coupling variables to (8) that enable obtaining the *decoupled* sub-problems for individual areas. Further, we include consistency constraints within each sub-problem to enforce agreement between adjacent areas on the values of coupling

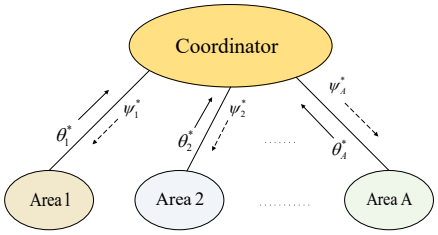

Fig. 2. Data exchange between areas and the coordinator.

variables. Let $\mathcal{B}_a$ be the set of boundary buses of area $a \in \mathcal{A}$ and associate to each bus $i \in \mathcal{B}_a$ the P-dimensional row vector of coupling variables $\boldsymbol{\psi}_{a,i}$. For $a \in \mathcal{A}$ and $(i,j) \in \mathcal{L}_a^{\text{tie}}$, the consistency constraints ensure the equality of voltage phase angle Bernstein coefficients and the corresponding coupling variables as

$$\boldsymbol{\theta}_{a,i} = \boldsymbol{\psi}_{a,i}, \quad \boldsymbol{\theta}_{a',j} = \boldsymbol{\psi}_{a',j}. \tag{9}$$

At each iteration r of the iterative algorithm, the following three steps are performed.

1) Solving Per-area Sub-problem (Step 1): Each area solves the following QP in iteration r:

$$\begin{aligned}\underset{\boldsymbol{\theta}_{a,i}^{(r)}, \boldsymbol{\theta}_{a',j}^{(r)}}{\text{minimize}} \quad & \mathcal{J}_a^{(\mathrm{r})} + \sum_{(i,j)\in\mathcal{L}_a^{\text{tie}}} \Big[\big(\boldsymbol{\theta}_{a,i}^{(\mathrm{r})} - \boldsymbol{\psi}_{a,i}^{\star(\mathrm{r}-1)}\big)\boldsymbol{\lambda}_{a,i}^{\star(\mathrm{r}-1)} \\ & + \frac{\rho}{2}\|\boldsymbol{\theta}_{a,i}^{(\mathrm{r})} - \boldsymbol{\psi}_{a,i}^{\star(\mathrm{r}-1)}\|_2^2 + \big(\boldsymbol{\theta}_{a',j}^{(\mathrm{r})} - \boldsymbol{\psi}_{a',j}^{\star(\mathrm{r}-1)}\big)\boldsymbol{\lambda}_{a',j}^{\star(\mathrm{r}-1)} \\ & + \frac{\rho}{2}\|\boldsymbol{\theta}_{a',j}^{(\mathrm{r})} - \boldsymbol{\psi}_{a',j}^{\star(\mathrm{r}-1)}\|_2^2 \Big] \qquad (10a) \\ \text{subject to} \quad & \text{Constraints } [(8b)\text{–}(8l)]_a \qquad (10b)\end{aligned}$$

where $\boldsymbol{\psi}_{a,i}^{\star(\mathrm{r}-1)}$ and $\boldsymbol{\psi}_{a',j}^{\star(\mathrm{r}-1)}$ are the optimal coupling variables calculated in Step 2 of iteration $r-1$, $\boldsymbol{\lambda}_{a,i}^{\star(\mathrm{r}-1)}$ and $\boldsymbol{\lambda}_{a',j}^{\star(\mathrm{r}-1)}$ are the updated dual variables calculated in Step 3 of the iteration $r-1$, and ρ is the step-size of dual update in Step 3.[1] The consistency constraints are enforced by forming the augmented Lagrangian in (10a), and $[(8b)\text{–}(8l)]_a$ represent the subset of constraints (8b)–(8l) pertinent to area a.

2) Optimizing Coupling Variables (Step 2): As shown in Fig. 2, each area obtains the optimal Bernstein coefficients $\boldsymbol{\theta}_{a,i}^{\star(r)}$ and $\boldsymbol{\theta}_{a',j}^{\star(r)}$ from the solution of (10) in Step 1 and sends them to the *coordinator* which, in turn, calculates the optimal coupling variables through the solution of following unconstrained optimization problem:

$$\begin{aligned}\underset{\boldsymbol{\psi}_{a,i}^{(r)}, \boldsymbol{\psi}_{a',j}^{(r)}}{\text{minimize}} \sum_{a\in\mathcal{A}} \sum_{(i,j)\in\mathcal{L}_a^{\text{tie}}} & \Big[\frac{\rho}{2}\big(\|\boldsymbol{\theta}_{a,i}^{\star(\mathrm{r})} - \boldsymbol{\psi}_{a,i}^{(\mathrm{r})}\|_2^2 + \|\boldsymbol{\theta}_{a',j}^{\star(\mathrm{r})} - \boldsymbol{\psi}_{a',j}^{(\mathrm{r})}\|_2^2\big) \\ & \big(\boldsymbol{\theta}_{a,i}^{\star(\mathrm{r})} - \boldsymbol{\psi}_{a,i}^{(\mathrm{r})}\big)\boldsymbol{\lambda}_{a,i}^{\star(\mathrm{r}-1)} + \big(\boldsymbol{\theta}_{a',j}^{\star(\mathrm{r})} - \boldsymbol{\psi}_{a',j}^{(\mathrm{r})}\big)\boldsymbol{\lambda}_{a',j}^{\star(\mathrm{r}-1)} \Big] \qquad (11)\end{aligned}$$

3) Updating Dual Variables (Step 3): For $a \in \mathcal{A}$ and $(i,j) \in \mathcal{L}_a^{\text{tie}}$, dual updates are performed as follows:

$$\boldsymbol{\lambda}_{a,i}^{\star(\mathrm{r})} = \boldsymbol{\lambda}_{a,i}^{\star(\mathrm{r}-1)} + \rho\big(\boldsymbol{\theta}_{a,i}^{\star(\mathrm{r})} - \boldsymbol{\psi}_{a,i}^{\star(\mathrm{r})}\big), \tag{12}$$

$$\boldsymbol{\lambda}_{a',j}^{\star(\mathrm{r})} = \boldsymbol{\lambda}_{a',j}^{\star(\mathrm{r}-1)} + \rho\big(\boldsymbol{\theta}_{a',j}^{\star(\mathrm{r})} - \boldsymbol{\psi}_{a',j}^{\star(\mathrm{r})}\big). \tag{13}$$

[1]Note that the starred values denote parameters of the optimization problem, not decision variables.

TABLE I
GENERATOR QUADRATIC COST FUNCTION COEFFICIENTS

Area	Generator	α[\$/(MWh)^2]	β[\$/MWh]	κ[\$]
1, 2	1	0.0042	9.11	0
1, 2	2	0.0152	6.86	0
1, 2	3	0.0275	1.55	0
3	1	0.0019	9.52	0
3	2	0.0122	5.41	0
3	3	0.0256	1.88	0

Algorithm stop condition: The iterative algorithm stops under the condition that $\forall a \in \mathcal{A},\ \forall (i,j) \in \mathcal{L}_a^{\text{tie}}$:

$$\text{abs}\big(\boldsymbol{\lambda}_{a,i}^{\star(\mathrm{r})} - \boldsymbol{\lambda}_{a,i}^{\star(\mathrm{r}-1)}\big), \text{abs}\big(\boldsymbol{\lambda}_{a',j}^{\star(\mathrm{r})} - \boldsymbol{\lambda}_{a',j}^{\star(\mathrm{r}-1)}\big) \ \leq \Delta\overline{\lambda} \tag{14}$$

where "abs" refers to absolute value and $\Delta\overline{\lambda}$ is a predetermined tolerable mismatch threshold.

III. NUMERICAL RESULTS

The distributed continuous-time OPF model proposed in Section II-C, as well as the centralized model in (8), are implemented on the three-area test network shown in Fig. 3, which is composed of identical areas except for cost functions of their generating units. For $a \in \{1,2,3\}$, the generation limits of units are $\underline{G}_a = [0,0,0]^{\mathrm{T}}$ and $\overline{G}_a = [600,400,200]^{\mathrm{T}}$ in [MW], and the ramp rate limits are $\dot{\overline{G}}_a = \dot{\underline{G}}_a = [100,65,80]^{\mathrm{T}}$ in [MW/hr]. The quadratic cost function coefficients of generators are reported in Table I and the transmission line/tieline data are provided in Table II. The 5-minute load data of California ISO (CAISO) [24] for March 19, 2023, is scaled down to a peak of 2850 [MW] and used to calculate the Bernstein coefficients of the continuous-time three-area network load shown in Fig. 4. The nodal loads of areas $a \in \{1,2,3\}$ are deemed of the same profile as the three-area network load, except scaled by factors $LF_a = [\frac{500}{2850}, \frac{300}{2850}, \frac{150}{2850}]^{\mathrm{T}}$.

A. Case 1: Adequate Ramping Resources

In this case adequate ramping resources are available and the generators are chiefly prioritized based on cost.

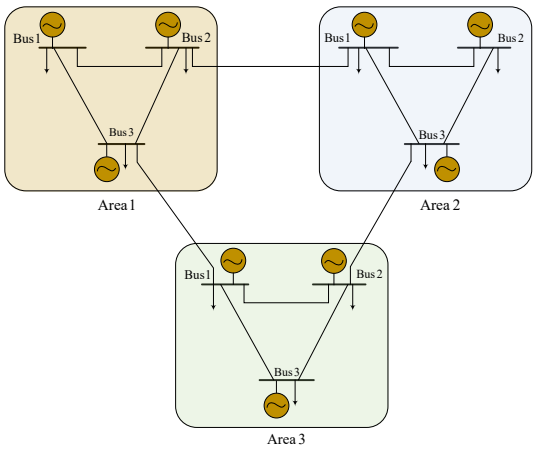

Fig. 3. One-line diagram of three-area test network.

TABLE II
TRANSMISSION LINE AND TIELINE DATA

Area	(i,j)	$x_{a,(i,j)}$[Ohm]	$\overline{F}_{a,(i,j)}$[MW]
$1,2,3$	$(1,2)$	0.01	200
$1,2,3$	$(1,3)$	0.02	120
$1,2,3$	$(2,3)$	0.01	200
Area	(i,j)	$x^{\text{tie}}_{a,(i,j)}$[Ohm]	$\overline{T}_{a,(i,j)}$[MW]
$1\rightarrow 2$	$(2,1)$	0.0161	75
$1\rightarrow 3$	$(3,1)$	0.0097	50
$2\rightarrow 3$	$(3,2)$	0.0104	50

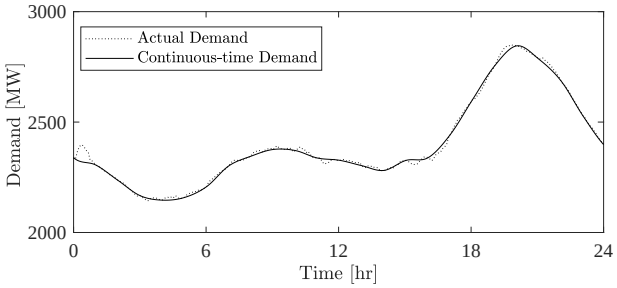

Fig. 4. Three-area network electricity demand.

1) Model Convergence: By choosing a stringent value of $\Delta\overline{\lambda} = 0.4$ and selecting $\rho = 60$, the ADMM converges in 120 iterations, and the total operation cost of the three areas smoothly approaches to that of the centralized model, as shown in Fig. 5. Initialized at 0, dual variables also near their steady-state values after roughly 20 iterations, as shown in Fig. 6, for two selected boundary buses (bus 1 of areas 2 and 3).

2) Optimal Trajectories: The generation trajectories of the generating units for all areas, obtained through distributed continuous-time OPF are presented in Fig. 7 as black traces.

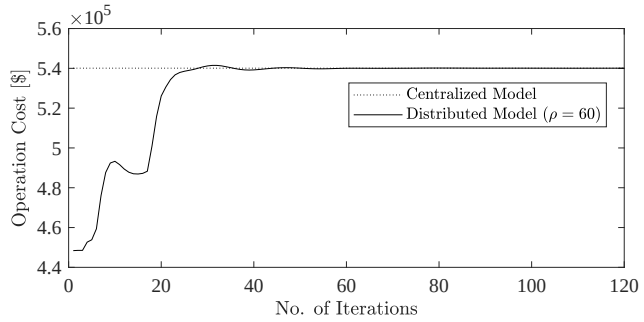

Fig. 5. Total operation cost of areas for distributed OPF model at each iteration of the ADMM for Case 1.

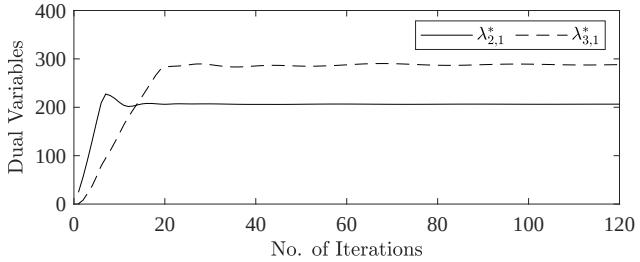

Fig. 6. Dual variables associated with two selected buses (bus 1 of areas 2 and 3) at each iteration of the ADMM for Case 1.

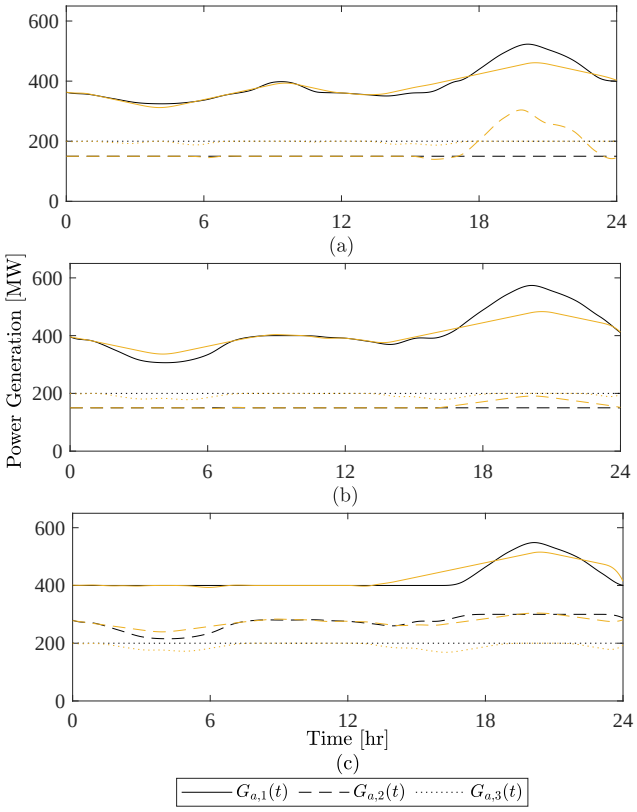

Fig. 7. Generation trajectories of generating units obtained from distributed continuous-time OPF for (a) $a = 1$, (b) $a = 2$, (c) $a = 3$. The black and orange traces refer respectively to Cases 1 and 2.

These trajectories coincide with that of centralized model except for an insignificant error. To evaluate this error, we integrate the absolute mismatch between optimal generation trajectories from distributed model, $G^{\star \text{d}}(t)$, and that of centralized model, $G^{\star \text{c}}(t)$, and average the resultant over all generators

$$ER^{\text{G}} = \frac{1}{\sum_{a\in\mathcal{A}} K_a} \int_{t\in\mathcal{T}} \sum_{a\in\mathcal{A}} \mathbb{1}^{\text{T}}_{K_a} \text{abs}\big(G^{\star \text{d}}(t) - G^{\star \text{c}}(t)\big) dt. \quad (15)$$

The ER^{G} amounts to a negligible value of 0.053 [MW].

The power flow of the tieline leaving bus 1 of area 3 is shown in Fig. 8, as a black trace, indicating its congestion except for $t \in [7,11]\cup[16,18]\cup[23,24]$. Tieline and transmission line power flows calculated from distributed OPF model also very closely follow the corresponding trajectories obtained from the centralized model where the pertinent errors are respectively $ER^{\text{tie}} = 0.11$ [MW] and $ER^{\text{line}} = 0.046$ [MW].

B. Case 2: Limited Ramping Resources

In this case, we synthesize an extreme case where ramping up and down limits of all generators are scaled down by a factor of 12 except for generator 2 of area 1 whose ramping limits are doubled. The generation schedule of generators deviate from that of Case 1, as shown in Fig. 1 with the orange traces. More precisely, the generator 2 of area 1, despite being

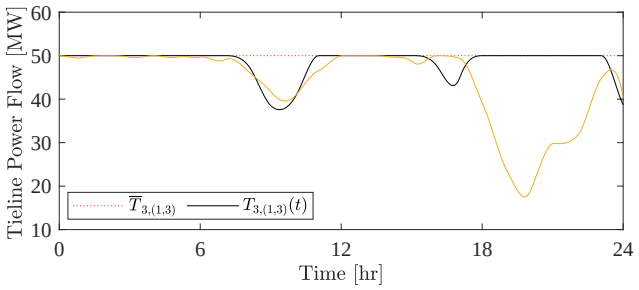

Fig. 8. Power flow of the tieline leaving bus 1 of area 3 obtained from distributed continuous-time OPF. The black and orange traces refer respectively to Cases 1 and 2, and the dotted red trace to the flow limit.

a relatively expensive resource, increases its power generation during peak-load hours to not only supply the nodal load ramping requirements in area 1, but also in areas 2 and 3. This reduces the tie-line power flow in Fig. 8, denoted in orange, during peak-load hours since the increased power generation of area 1 induces a power flow component in the opposite direction to that in Case 1. The numerical results in Case 2 highlight the efficiency of distributed continuous-time OPF to leverage ramping resources of area 1 (with excess ramping) to address the ramping scarcity of other areas.

C. Computation Time

The proposed distributed solution of the continuous-time OPF problem is implemented in GAMS optimization platform and solved using the CONOPT4 solver on a desktop computer with a 3.70 [GHz] i9 CPU and 32 [GB] RAM. The ADMM converges in 55 [sec] and 102 [sec] respectively for Cases 1 and 2 which is favorable for day-ahead scheduling. The model is expected to suitably scale for the case of areas embedding larger networks as the computation time of QP problems in (10), attributed to individual areas, would not considerably increase for real-world network sizes. In addition, since the real-world interconnected networks typically incorporate a limited number of areas which solve (10) in parallel, the case of increased number of areas would also remain computationally manageable.

IV. Concluding Remarks and Future Work

In this paper, we proposed a distributed continuous-time OPF model for a multi-area transmission network. The proposed approach enabled a higher-precision modeling of system load and generation trajectories by first formulating a continuous-time variational optimization problem, and then projecting it into the Bernstein function space and decomposing it to individual area sub-problems using the ADMM. The model is implemented on a synthesized three-area test network where the simulation results showcase the effective convergence to the optimal solution of the benchmark centralized model, and the efficient sharing of ramping resources among areas. Future work includes the extension to unit commitment problem, incorporating energy storage and flexible loads, and accounting for load uncertainty.

References

[1] B. Kroposki, "Integrating high levels of variable renewable energy into electric power systems," *Journal of Modern Power Syst. and Clean Energy*, vol. 5, no. 6, pp. 831–837, Nov. 2017.

[2] R. L. Graham, J. Francis, and R. J. Bogacz, "Challenges and opportunities of grid modernization and electric transportation," US Department of Energy and Allegheny Science & Technology, Tech. Rep., 2017.

[3] L. Bird, M. Milligan, and D. Lew, "Integrating variable renewable energy: Challenges and solutions," National Renewable Energy Lab., Golden, CO, Tech. Rep., 2013.

[4] M. Muratori and T. Mai, "The shape of electrified transportation," *Environmental Research Letters*, vol. 16, no. 1, p. 011003, 2020.

[5] J. Katz and J. Cochran, "Integrating variable renewable energy into the grid: Key issues, greening the grid," National Renewable Energy Lab., Golden, CO, Tech. Rep., 2015.

[6] A. J. Wood, B. F. Wollenberg, and G. B. Sheblé, *Power generation, operation, and control*. John Wiley & Sons, 2013.

[7] M. Parvania and A. Scaglione, "Unit commitment with continuous-time generation and ramping trajectory models," *IEEE Trans. on Power Syst.*, vol. 31, no. 4, pp. 3169–3178, Jul. 2016.

[8] R. Khatami, M. Parvania, and P. P. Khargonekar, "Scheduling and pricing of energy generation and storage in power systems," *IEEE Trans. on Power Syst.*, vol. 33, no. 4, pp. 4308–4322, Jul. 2018.

[9] R. Khatami and M. Parvania, "Stochastic multi-fidelity scheduling of flexibility reserve for energy storage," *IEEE Trans. on Sust. Energy*, vol. 11, no. 3, pp. 1438–1450, Jul. 2020.

[10] R. Khatami, M. Parvania, C. Chen, S. S. Guggilam, and S. V. Dhople, "Dynamics-aware continuous-time economic dispatch: A solution for optimal frequency regulation." in *53rd Hawaii Int. Conf. on Syst. Sciences*, 2020, pp. 1–10.

[11] R. Khatami, M. Parvania, and P. Khargonekar, "Continuous-time look-ahead scheduling of energy storage in regulation markets," in *52nd Hawaii Int. Conf. on Syst. Sciences*, 2019, pp. 3598–3606.

[12] C. Ø. Naversen, M. Parvania, A. Helseth, and H. Farahmand, "Continuous hydrothermal flexibility coordination under wind power uncertainty," *IEEE Trans. on Sust. Energy*, vol. 13, no. 4, pp. 1900–1912, Oct. 2022.

[13] A. Nikoobakht, J. Aghaei, M. Shafie-Khah, and J. P. Catalão, "Continuous-time co-operation of integrated electricity and natural gas systems with responsive demands under wind power generation uncertainty," *IEEE Trans. on Smart Grid*, vol. 11, no. 4, pp. 3156–3170, Jul. 2020.

[14] M. Majidi, E. Davoodi, B. Li, B. Mohammadi-Ivatloo, and M. Parvania, "Continuous-time day-ahead operation of multienergy systems," *IEEE Syst. Journal*, vol. 15, no. 4, pp. 5595–5605, Dec. 2021.

[15] A. Kargarian, J. Mohammadi, J. Guo, S. Chakrabarti, M. Barati, G. Hug, S. Kar, and R. Baldick, "Toward distributed/decentralized DC optimal power flow implementation in future electric power systems," *IEEE Trans. on Smart Grid*, vol. 9, no. 4, pp. 2574–2594, Jul. 2018.

[16] A. R. Malekpour, A. Pahwa, and B. Natarajan, "Hierarchical architecture for integration of rooftop pv in smart distribution systems," *IEEE Trans. on Smart Grid*, vol. 9, no. 3, pp. 2019–2029, May 2018.

[17] F. Safdarian and A. Kargarian, "Temporal decomposition-based stochastic economic dispatch for smart grid energy management," *IEEE Trans. on Smart Grid*, vol. 11, no. 5, pp. 4544–4554, Sep. 2020.

[18] A. Garcia, R. Khatami, C. Eksin, and F. Sezer, "An incentive compatible iterative mechanism for coupling electricity markets," *IEEE Trans. on Power Syst.*, vol. 37, no. 2, pp. 1241–1252, Mar. 2022.

[19] Á. Paredes, J. A. Aguado, and P. Rodríguez, "Uncertainty-aware trading of congestion and imbalance mitigation services for multi-DSO local flexibility markets," *IEEE Trans. on Sust. Energy*, Mar. 2023.

[20] Q. Zhang, Y. Guo, Z. Wang, and F. Bu, "Distributed optimal conservation voltage reduction in integrated primary-secondary distribution systems," *IEEE Trans. on Smart Grid*, vol. 12, no. 5, pp. 3889–3900, Sep. 2021.

[21] S. Talari, S. Birk, W. Ketter, and T. Schneiders, "Sequential clearing of network-aware local energy and flexibility markets in community-based grids," *IEEE Trans. on Smart Grid*, May 2023.

[22] A. G. Bakirtzis and P. N. Biskas, "A decentralized solution to the DC-OPF of interconnected power systems," *IEEE Trans. on Power Syst.*, vol. 18, no. 3, pp. 1007–1013, Aug. 2003.

[23] P. M. Prenter *et al.*, *Splines and variational methods*. Courier Corporation, 2008.

[24] California ISO Operan Access Same-Time Information System, March. 2023. [Online]. Available: http://oasis.caiso.com